Title
Retinal Representation of the Elementary Visual Signal

Permalink
https://escholarship.org/uc/item/3h32w05j

Journal
Neuron, 81(1)

ISSN
0896-6273

Authors
Li, Peter H
Field, Greg D
Greschner, Martin
et al.

Publication Date
2014

DOI
10.1016/j.neuron.2013.10.043

Peer reviewed

Retinal representation of the elementary visual signal

Peter H. Li[1,*], **Greg D. Field**[1,2], **Martin Greschner**[1,3], **Daniel Ahn**[1], **Deborah E. Gunning**[4], **Keith Mathieson**[4], **Alexander Sher**[5], **Alan M. Litke**[5], and **E.J. Chichilnisky**[1,6]

[1]Systems Neurobiology Laboratories, Salk Institute for Biological Studies, La Jolla, California 92037

[2]Zilkha Neurogenetic Institute, Department of Cell and Neurobiology, Keck School of Medicine, University of Southern California, Los Angeles, California 90033

[3]Department of Neuroscience, Carl von Ossietzky University, 26129 Oldenburg, Germany

[4]Institute of Photonics, University of Strathclyde, Glasgow, G4 0NW, United Kingdom

[5]Santa Cruz Institute for Particle Physics, University of California, Santa Cruz, California 95064

[6]Department of Neurosurgery, School of Medicine, Stanford University, Palo Alto, California 94305

Summary

The propagation of visual signals from individual cone photoreceptors through parallel neural circuits was examined in the primate retina. Targeted stimulation of individual cones was combined with simultaneous recording from multiple retinal ganglion cells of identified types. The visual signal initiated by an individual cone produced strong responses with different kinetics in three of the four numerically dominant ganglion cell types. The magnitude and kinetics of light responses in each ganglion cell varied nonlinearly with stimulus strength, but in a manner that was independent of the cone of origin after accounting for the overall input strength of each cone. Based on this property of independence, the receptive field profile of an individual ganglion cell could be well estimated from responses to stimulation of each cone individually. Together these findings provide a quantitative account of how elementary visual inputs form the ganglion cell receptive field.

Introduction

In the visual system, the elementary sensory signal is transduction of light in a retinal photoreceptor cell. Parallel circuits process and transform this signal into spatiotemporal patterns of activity in retinal ganglion cells (RGCs), which are then transmitted to the brain and mediate visual function (Sterling and Demb, 2004; Wassle, 2004; Nassi and Callaway, 2009). Many studies have shown that light absorption by one or a few rod photoreceptors can drive downstream physiological signals and visual behavior in night vision (see Field et al., 2005). It also appears that in daylight vision the signals from individual cone photoreceptor signals can be detected centrally (Hofer et al., 2005; Sincich et al., 2009), noise in cone signals may limit visual fidelity (Ala-Laurila et al., 2011), and the

*To whom correspondence may be addressed: peterli@salk.edu; peter.hawley.li@gmail.com.

representation of space is precise at the level of individual cones (Chichilnisky and Baylor, 1999; Field et al., 2010).

However, fundamental questions remain about the signal arising from a single cone. What is the strength of this elementary signal in the downstream parallel pathways of the primate visual system? Do the specialized visual representations in different pathways arise from differential processing of elementary signals? How do the signals from different cones contribute to forming the spatial structure, kinetics and nonlinearities in receptive fields of downstream neurons? Ultimately, these questions pertain not only to visual or sensory systems, but to the processing and representation of elementary signals in neural circuits generally.

We examined the activity produced at the output of the primate retina by selective visual stimulation of individual cone photoreceptors, and how this activity depends on stimulus strength, on the particular cone stimulated, and on the flow of visual signals through parallel retinal circuits. The results establish the basic properties of the elementary visual signal and how they shape the retinal output.

Results

To probe the elementary signal, light responses of RGCs were recorded from peripheral primate retina *ex vivo* using a high-density 512-electrode array (Chichilnisky and Baylor, 1999; Litke et al., 2004; Frechette et al., 2005; Field et al., 2010). The light responses of each RGC were first characterized at a coarse spatial scale by stimulating the retina with spatiotemporal noise and computing the spike-triggered average stimulus (see Experimental Procedures). This characterization was performed at an intensity that modulated cone signals but kept the rods in saturation (Rodieck, 1998). Several features of the spike-triggered average, including spatial receptive field size and response dynamics, were used to identify the four numerically dominant ganglion cell types: ON and OFF midget, and ON and OFF parasol.

The receptive fields of these cells were then measured at high resolution using spatiotemporal noise with small pixels. This characterization revealed punctate islands of light sensitivity within each receptive field (Fig. 1A), which correspond to the locations of individual cones in the photoreceptor mosaic (Field et al., 2010). High resolution receptive fields of many RGCs were then combined during ongoing recording to produce a local map of the cone mosaic (Fig. 1B and see Experimental Procedures). Over some regions, the regular spacing of identified cones within the map indicated that it was nearly complete.

Single cone response magnitude and divergence

To explore the visual signal initiated by individual cones, the cone mosaic map was then used to design second-pass high resolution stimuli, in which small regions of the display were selected to illuminate single cones without illuminating neighbors (e.g. Fig. 2, black polygonal outlines). Brief steps of light were presented within these regions, as increments or decrements from a uniform gray field, while recording the activity of RGCs. Long- and middle-wavelength sensitive cones were primarily targeted; short-wavelength sensitive cones provide at most weak input to the RGC types tested (Field et al., 2010).

Single cone stimulation produced robust patterns of firing in RGCs, with single trial responses often clearly discriminable from baseline firing (Fig 2). Strong responses were routinely observed in OFF midget and OFF parasol cells. ON midget cells generally responded somewhat more weakly (Fig. 2, right column), while the ON parasol cells tested

did not respond reliably to single cone stimulation (see Discussion). In what follows, analysis will be focused on ON and OFF midget cells and OFF parasol cells.

Signals from a single cone diverged to drive firing in more than one recorded RGC simultaneously (Fig. 3). The observed signal divergence was consistent with the apparent overlap of receptive fields obtained from spatiotemporal noise stimulation at single cone resolution (Field et al., 2010). Because RGCs of the same type exhibited relatively little receptive field overlap (Devries and Baylor, 1997; Gauthier et al., 2009; Field et al., 2010), the observed examples of divergence were most pronounced in RGCs of different types.

Cones contributing to RGC receptive field surround regions were only weakly detectable in receptive field maps measured with spatiotemporal noise. However, the locations of cones in the receptive field surround could be inferred from the receptive field centers of neighboring RGCs. Stimulation of these surround cones resulted in weaker RGC responses, of opposite polarity (Fig. 3, lower right panels).

Nonlinearity and univariance of single cone responses

Different cone inputs to a given RGC typically elicited responses of different magnitude and kinetics, even when the stimulus contrast was the same (Fig. 2). Does every cone drive the RGC with unique contrast response and kinetics? This possibility would complicate the interpretation of measurements of synaptic strength and plasticity. A simpler possibility would be that the cones providing input to a RGC vary only in the overall strength of their input, but otherwise produce identical responses.

To test this possibility, responses were measured as a function of contrast for each of four selected cone inputs to a given RGC. Response to single cone stimulation increased nonlinearly with contrast, following an accelerating form suggesting thresholding and noise in the retinal circuitry and consistent with previous findings (Chichilnisky and Kalmar, 2002).

To determine whether the response nonlinearity associated with different cones had a common form, the contrast axes for the four input cones were rescaled to allow for differences in cone input strength. After rescaling, these functions superimposed closely (Fig. 4A), suggesting equivalent nonlinear response characteristics. Residual deviations after rescaling were 0.9–6.5% of the maximum response amplitude across 47 RGCs tested (Fig. 4B). To test whether the kinetics of response were also equivalent, responses elicited by stimulation of different cones but producing roughly equal response magnitude in a given RGC were compared (Fig. 4A, bottom panel insets). The dynamics of these responses matched closely, even though the stimulus contrast eliciting them often differed significantly (e.g. Fig. 4A left panels). Thus, after normalizing for the overall input strength of each cone, RGC contrast response and kinetics were independent of the cone of origin (that is, they were *univariant*; see Discussion).

Origins of midget and parasol response specializations

Different RGC types exhibit diverse response properties, e.g. the well-established higher contrast sensitivity and more transient light responses in parasol compared to midget cells (Gouras, 1968; Kaplan and Shapley, 1986; Croner and Kaplan, 1995; Lee et al., 1989). How do these specializations come about? A simple possibility is that these differences arise from the processing of elementary cone signals via the retinal circuitry, and thus are evident in RGC responses to single cone stimulation.

To probe the origin of differences in contrast sensitivity, OFF midget and OFF parasol response amplitudes were compared as a function of contrast using single cone stimulation.

This measurement generally revealed similar contrast sensitivity in the two cell types, with slightly higher sensitivity in midget cells in some recordings (Fig. 5A). Thus the greater contrast sensitivity of parasol cells under stimulation at larger spatial scales apparently does not derive from the processing of individual cone signals in the retinal circuitry.

Alternatively, the difference in contrast sensitivity could arise from the convergence of a larger number of cone inputs to parasol cells than midget cells (Kaplan et al., 1990). To test this possibility, the response of each RGC to stimulation of the entire receptive field center was estimated from the contrast-response function of a single cone within the receptive field (Fig. 5A), scaled on the contrast axis by the fraction of the total input to the RGC provided by that cone, as estimated from receptive field maps obtained by reverse correlation (e.g., Figs. 1, 2, 3; see Discussion). This calculation produced contrast-response functions that were significantly steeper for parasol than midget cells (Fig. 5B), consistent with previous findings using coarser stimuli. The distribution of estimated contrast gains (initial slopes of contrast-response functions) for individual midget and parasol cells also resembled the distribution of contrast gains previously observed with drifting grating stimuli (Fig. 5C) (Kaplan and Shapley, 1986). Thus, the higher contrast sensitivity of OFF parasol cells relative to OFF midget cells may be a consequence of the difference in the number of cones providing input to cells of the two types (Kaplan et al., 1990).

Although single cone stimulation did not yield reliable responses in ON parasol cells, simultaneous stimulation of two cones in ON midget and ON parasol cells yielded similar or slightly higher sensitivity in midget cells (not shown), consistent with the results of single-cone analysis in OFF midget and OFF parasol cells (see Discussion).

To probe the origin of differences in response kinetics between midget and parasol cells, the time course of response to single cone stimulation was compared. The response was notably more transient in parasol cells (Figs. 2 and 3). Furthermore, the kinetics of single cone responses were approximately predicted by the convolution of the light step time course with the impulse response of the RGC inferred from large-scale spatiotemporal noise stimulation, in both midget and parasol cells (not shown) (Chichilnisky, 2001). Thus, the distinction between sustained and transient classes of RGCs does not depend on the aggregation of cone signals over space, but arises from retinal processing of individual cone signals (see Discussion).

Correspondence of cone input strength measures

Previous work has characterized the receptive fields of midget and parasol RGCs in primate retina using reverse correlation with high resolution spatiotemporal noise stimuli (Field et al., 2010). This approach provides a rapid quantitative summary of cone input strength across the receptive field. Given the significant known nonlinearities in RGCs (e.g. Hochstein and Shapley, 1976; Shapley and Victor, 1981), how accurately does this linear approximation capture the strength of cone inputs? A simple possibility is that the nonlinearities in RGC responses are of a form and magnitude that permit approximately veridical estimates of cone input strengths using spatiotemporal noise (e.g. see Chichilnisky, 2001).

To test this possibility, the finding of univariance was exploited to obtain an estimate of the relative input strength of every cone in the receptive field. First, for each cone, a single scale factor was identified that, when multiplied by the contrast of the stimulus presented to that cone, brought its contrast-response function into register with the contrast-response functions of the other cones (see Fig. 4). Because this factor effectively rescaled the stimulus, it was taken to indicate the relative strength of the input from that cone. The collection of scale factors obtained this way from every cone produced a spatial map of cone

input strength (Fig. 6B–F, top). This map was then compared to the cone input strength map inferred from reverse correlation with spatiotemporal noise stimuli (Fig. 6B–F, bottom). The cone input strength maps obtained using the two approaches were similar in these examples and in aggregate (Fig. 6G), although small discrepancies were visible (see Discussion). Across 21 OFF midget cells tested, the median R^2 value relating the cone strength values obtained with the two methods was 0.80. Therefore, despite the nonlinear responses to stimulation of individual cones, receptive field maps obtained with spatiotemporal noise provided a roughly accurate description of the relative strength of input from each cone to each RGC.

Discussion

The structure of the activity in RGCs produced by stimulation of a single cone generally followed simple rules. Signals from each cone diverged to parallel retinal circuits, producing robust responses in at least three major RGC types, with similar magnitude but different kinetics in OFF midget and OFF parasol cells. For a given RGC, the contrast-response and kinetics of light responses initiated by different cones were similar, yielding an effectively *univariant* light response. Differences in contrast sensitivity between midget and parasol cells were mostly attributable to cone convergence, whereas differences in response kinetics arose from processing of individual cone signals. The relative strengths of isolated inputs from different cones were well approximated by the input strength estimated using reverse correlation with high resolution spatiotemporal noise.

Strength and divergence of the elementary visual signal

The divergence of signals from individual cones to multiple parallel circuits in the retina was strongly predicted from anatomical work showing that each cone feeds multiple bipolar cells of different types (Grunert et al., 1994; Chun et al., 1996). Recently, this prediction was reinforced in physiological recordings from complete populations of the four major primate RGC types, revealing the locations of individual cones in their receptive fields (Field et al., 2010). In that work, each of the four major RGC populations effectively sampled the entire mosaic of L and M cones over a region of the retina, implying that in general each cone provided input to each of the four cell types. The current results on divergence (Fig. 3) confirm these predictions and provide insight into the factors controlling response magnitude and kinetics in the different RGC types.

The observation of robust RGC responses to stimulation of an individual photoreceptor has some precedent. A large body of work indicates that absorption of one or a few photons in rod photoreceptors can drive reliable visual signals in RGCs, and can mediate effective stimulus detection in humans (see Field et al., 2005). However, cones exhibit much lower unitary photovoltages than rods (Schneeweis and Schnapf, 1995), and their signals are transmitted to RGCs by distinct circuitry under distinct adaptation conditions. Thus, a stronger prediction comes from anatomical work showing that in the foveal region of the retina midget RGCs receive input from only one cone (Wassle et al., 1994; Kolb and Marshak, 2003). Presumably, then, foveal midget cells can be strongly driven by one cone, and indeed behavioral evidence indicates that single cone stimulation in central retina can produce reliable visual percepts (Hofer et al., 2005; Sincich et al., 2009).

However, at the peripheral retinal eccentricities sampled here, midget cells typically received significant input from 5–15 cones while parasol cells received significant input from 40–80 cones (Fig. 1). Thus, the present results demonstrate that even a cone that forms a relatively small fraction of the total input to a RGC can drive strong light responses in that cell. These findings are consistent with work in turtle retina indicating that electrical stimulation of a single cone yields robust firing in a RGC (Baylor and Fettiplace, 1977); in

this work the number of cones in the receptive field was not measured but was probably larger than in primate midget cells. More recently, electrical stimulation of individual cones in primate retina was shown to drive significant synaptic currents in parasol cells (Ala-Laurila et al., 2011). The present findings are also consistent with currents evoked in salamander RGCs by stimuli illuminating 1–2 cones (Soo et al., 2011), although again the number of cones feeding the RGCs was not reported.

Reliable single-cone responses were not observed in ON parasol cells, which have the largest number of cone inputs of the RGC types tested, although responses to simultaneous stimulation of cone pairs were robust in some cases (not shown). It remains to be determined whether this finding reflects different sensitivity in ON-parasol cells or limitations of the experimental preparation. Recent findings indicate that primate cones themselves respond more weakly to high-contrast increments than to high-contrast decrements (J. Angueyra & F. Rieke, personal communication), which may help explain the weaker responses in ON compared to OFF RGCs observed here, given that they were primarily targeted with matched polarity stimuli. This fact, coupled with the tendency toward slightly lower single-cone sensitivity in parasol compared to midget cells (Fig. 5A), may explain the weak single cone responses in ON parasol cells relative to the other cell types.

In principle, cone-cone gap junction coupling (Hornstein et al., 2004) could contribute to divergence of single cone signals. The results of Fig. 3 suggest, however, that this effect is not large. For example, strong cones in receptive field center regions were observed immediately adjacent to known locations of cones that provided no discernible input, while cones in the receptive field surround generated robust responses of opposite polarity. However, the possibility of sporadic or non-isotropic cone coupling in some cases cannot be excluded.

Univariant light responses in retinal ganglion cells

In principle, the multiple cone inputs driving responses in a RGC could produce signals with distinct properties. For example, different cones could drive a given RGC with different response time course, or a different dependence on stimulus contrast, depending on the specific retinal interneurons involved in conveying their signals to the RGC. If this were true, the receptive field of the RGC could exhibit complex properties not easily summarized by a single spatial sensitivity profile, response time course, or dependence on contrast, with important implications for retinal circuitry and for models of visual function.

A simpler hypothesis is that signals from different cones are stereotyped and effectively equivalent in the way they drive RGC responses, except for differences in overall strength. This possibility is suggested by the largely homogeneous mosaics of bipolar cells that convey signals from cones to each distinct RGC type: presumably, bipolar cells of each type exhibit stereotyped response properties; therefore, inputs from different cones may vary only in their strength. It is also suggested by previous studies indicating approximate space-time separability in the RGC receptive field center (see e.g. Enroth-Cugell et al., 1983; Dawis et al., 1984; Chichilnisky and Kalmar, 2002), i.e. the idea that to a first approximation, the spatiotemporal receptive field can be described as the product of independent spatial and temporal sensitivity profiles. However, separability observed in preceding work was approximate, was observed only at a coarse spatial scale, and depended on a linear model that does not fully capture the properties of RGC light response.

The concept of equivalence of signals from different sources has an important precedent in color vision and photoreceptor physiology: the term *univariance* refers to the idea that despite nonlinearities, lights of different wavelength drive responses with the same time course and dependence on stimulus strength, once the probability of absorption is taken into

account (Naka and Rushton, 1966b; Naka and Rushton, 1966a; Baylor et al., 1987). By extension, the hypothesis tested here was that the responses of RGCs are univariant with respect to the cone of origin, i.e. that all cones in the receptive field center of a given RGC produce equivalent responses, once the input strength associated with the cone is taken into account. Univariance of cone inputs would provide a simple picture of the RGC receptive field center that is often implicitly assumed but little tested.

The present results strongly support univariance. The nonlinear dependence of response on contrast and the overall kinetics of responses in each RGC were independent of the cone of origin, except for a single overall scale factor that reflected the efficacy of signals from each cone in driving responses (Fig. 4). This held in the receptive field centers of both midget and parasol cells, despite their distinct upstream circuitry and receptive field properties. Consistent with previous work (Gouras and Zrenner, 1979; Smith et al., 1992), however, this property likely does not hold between the receptive field center and surround; responses to surround cone stimulation generally could not be overlaid on center cone responses simply by applying a negative scale factor (not shown).

Sensitivity and dynamics of cone inputs to midget and parasol cells

The magnitude of individual cone responses measured in OFF midget and OFF parasol cells was similar, or in some cases slightly lower in parasol cells (e.g. Fig. 5A, bottom). While these results do not point to specific mechanisms controlling contrast gain between individual cones and RGCs, they are somewhat surprising in light of previous work showing substantially higher contrast sensitivity in parasol compared to midget cells (Kaplan and Shapley, 1986; Croner and Kaplan, 1995; Lee et al., 1989). However, previous measurements of contrast sensitivity were typically obtained with larger-scale stimuli, such as sinusoidal gratings with a spatial period comparable to the receptive field size of the recorded cells.

A hypothesis which reconciles the previous and current findings is that each cone is on average nearly equally effective at driving activity in midget and parasol cells, but the latter receive input from more cones and therefore exhibit higher contrast sensitivity to large stimuli (Kaplan et al., 1990). This hypothesis was tested by estimating contrast sensitivity weighted and summed over all the cones in the receptive field. These estimates relied on the validity of relative cone input strengths obtained from receptive field maps, which was confirmed in midget cells (Fig. 6; see below), and on the assumption of approximately linear spatial summation within the receptive field prior to any nonlinearity in response. On average, the resulting contrast gain was roughly 6 times higher in parasol cells than midget cells (Fig. 5B, heavy lines), consistent with sensitivity differences previously reported (Kaplan and Shapley, 1986; Croner and Kaplan, 1995; Lee et al., 1989). Furthermore, the distribution of contrast gains for the populations of midget and parasol cells resembled the distribution of contrast gains previously reported (Fig. 5C) although the gain scales differed, probably in part due to differences in stimulus conditions. Thus the greater contrast sensitivity of parasol compared to midget RGCs is largely explained by the larger number of cone inputs to parasol cells.

Differences in response dynamics between midget and parasol cells (Gouras, 1968) could not be explained this way. Parasol cells exhibited a more transient time course of response to single cone stimulation than midget cells (Figs. 2, 3). Thus, kinetic differences are not attributable to greater convergence, but instead are intrinsic to the processing of elementary cone signals. This finding is consistent with work revealing diverse response kinetics in different bipolar cell types (DeVries, 2000; Baden et al., 2013).

Interpretation of receptive field structure in retinal ganglion cells

The spatial structure of the mammalian RGC receptive field has been measured and summarized in many studies and species, starting with seminal work in cat retina (Kuffler, 1953). Ultimately, the receptive field is composed of inputs from multiple photoreceptors, and receptive field sensitivity profiles must reflect the strength and spatial structure of photoreceptor inputs. To measure receptive fields, many studies have adopted the technique of reverse correlation with spatiotemporal noise stimuli, because of its technical advantages (see Marmarelis and Marmarelis, 1978; Chichilnisky, 2001). Recently, high resolution receptive field maps obtained by reverse correlation with fine-grained spatiotemporal noise were used to obtain estimates of the relative strength of all the cone inputs to each RGC (Field et al., 2010). This approach raises a question relevant for all neuronal receptive field estimates: how accurately do they reflect the strength of the individual, elementary inputs?

The univariance of RGC signals with respect to the cone of origin suggests a natural and well-defined measure of relative cone input strength: the scale factor required to bring the contrast-response curves and response time course from different cones into register. The similarity between this measure of cone input strength and the results obtained with reverse correlation (Fig. 6) confirm that the latter provide largely accurate estimates of cone input strength across the RGC receptive field.

Although the success of reverse correlation in predicting the strength of cone inputs would be broadly consistent with a linear spatial summation of cone signals by midget RGCs, there are other possibilities. For example, a half-wave rectification of each cone input would yield the same result while violating linear summation. Furthermore, the data in Fig. 6G reveal slight deviations from the unity line. The compressive form of the deviation indicates that for the weaker cones in the receptive field, cone strengths estimated from spatiotemporal noise tend to be relatively lower than those estimated from stimulation of single cones. Such discrepancies could be due to nonlinear spatial summation (e.g. Hochstein and Shapley, 1976; Victor and Shapley, 1979; Demb et al., 1999; Bolinger and Gollisch, 2012; Schwartz et al., 2012), but could also arise in part from the fact that the spatiotemporal noise stimulus was binary rather than Gaussian (e.g. see Chichilnisky, 2001). Additional stimulus configurations (see J. Freeman *et al.*, in preparation) will be needed to distinguish linear summation of cone signals from other possibilities, such as linear combination into subunits that combine nonlinearly to drive RGC firing.

The present work provided limited analysis of cone signals from the antagonistic surround region of RGC receptive fields (Kuffler, 1953). However, these techniques in principle permit further analysis, by identifying the locations of surround cones based on the receptive field centers of neighboring RGCs simultaneously recorded (Fig. 3). Thus, future work could investigate the kinetics and summation of cone signals across the entire receptive field, with implications for the mechanisms and retinal circuitry underlying surround antagonism within and across RGC types.

The property of univariance (Fig. 4) and the validation of a linear approximation of input strengths (Fig. 6) are powerful simplifying principles for the efficient characterization and modeling of neural circuits. Without an assumption of univariance, many prevailing descriptions of neuronal connection strengths and plasticity lack straightforward interpretations or generalizability. The current results validate the univariance assumption in the context of the primate retina, and suggest approaches to test its validity in other neuronal circuits.

Experimental Procedures

Electrophysiological recording and visual stimulus

Preparation and recording methods were described previously (Chichilnisky and Kalmar, 2002; Frechette et al., 2005; Field et al., 2010). Eyes were enucleated from nine terminally anesthetized macaque monkeys (*Macaca sp.*) used by other experimenters in accordance with institutional guidelines for the care and use of animals. Most animals were in good health. Some had been used for behavioral and neurophysiological experiments, others had been experimentally exposed to drugs of addiction, and one had been terminally anesthetized for several days. No systematic differences in retinal physiology were observed between categories of animals. Immediately after enucleation, the anterior portion of the eye and the vitreous were removed in room light. Segments of peripheral retina (eccentricity 5.5–13.8 mm temporal equivalent (Chichilnisky and Kalmar, 2002)) were dissected and placed flat, RGC side down, on a planar array of extracellular microelectrodes. The array consisted of 512 electrodes in an isosceles triangular lattice with 30 μm spacing, covering a hexagonal region 450 μm on a side. Attachment to the pigment epithelium was preserved during dissection. In some preparations the choroid was largely removed, up to Bruch's membrane, to ensure even retinal thickness and maximize oxygenation. While recording, the retina was perfused with Ames' solution (31–36 °C) bubbled with 95% O2 and 5% CO2, pH 7.4.

Recordings were analyzed online to isolate the spikes of different cells, as described previously (Litke et al., 2004; Field et al., 2007). Briefly, candidate spike events were detected using a threshold on each electrode, and voltage waveforms on the electrode and nearby electrodes around the time of the spike were extracted. Clusters of similar spike waveforms were identified as candidate neurons if they exhibited a 1 ms refractory period and comprised more than 100 spikes. Duplicate recordings of the same cell were identified by temporal cross-correlation and removed.

Visual stimulation was performed with the optically reduced image of a gamma-corrected OLED microdisplay (eMagin, Bellvue, WA) refreshing at 60.35 Hz focused on the photoreceptor outer segments. The emission spectrum of each display primary was measured with a spectroradiometer (PR-701, PhotoResearch, Chatsworth, CA) after passing through the optical elements between the display and the retina. The mean photoisomerization rates for the L, M and S cones were estimated by computing the inner product of the power scaled emission spectra per unit area with the spectral sensitivity of each opsin, and multiplying by the effective collecting area of primate cones ($0.37 \mu m^2$) (Baylor et al., 1987). The power of each display primary was measured at the preparation with a calibrated photodiode (UDT Instruments, San Diego, CA). At the mean background illumination level, the photoisomerization rates for the rods, L, M, and S cones were approximately 29120, 9440, 9270, and 2320 photoisomerizations per receptor per second. These estimates were not corrected for the angle of illumination and pigment self screening in the cone outer segments, because the precise angle of illumination and the amount of bleached pigment were unknown. For a few points in Fig. 6G, neutral density filters reduced the stimulus intensity by approximately four-fold; no systematic difference was observed.

Spatiotemporal noise stimulus and analysis

The spatial, temporal and chromatic response properties of recorded RGCs were characterized using a spatiotemporal noise stimulus, composed of a lattice of square pixels updating randomly and independently of one another over time (see Chichilnisky, 2001). For initial characterization with large pixels, the intensity of each display primary at each pixel location was chosen from a binary distribution at each refresh, independent of the other

primaries, yielding a stimulus with chromatic variation. For high resolution characterization of individual cones, the intensities of the display primaries were modulated in unison, yielding an achromatic binary intensity modulation with higher variance and thus greater modulation of RGC responses. In both conditions, the contrast of each primary (difference between the maximum and minimum intensities divided by the sum) was 96%. For low spatial resolution receptive field maps used for classification (not shown), the pixels were 25.5 or 34 μm on a side, the stimulus refresh rate was 20, 30, or 60 Hz, and recording duration was 30 minutes. For high resolution maps (Figs. 1A, 2, 3, 6A), the pixels were 3.4 μm on a side, the stimulus refresh rate was 10, 12, or 15 Hz, and recording duration was 30–60 minutes.

For online cell type classification, receptive fields were summarized by independently fitting the spatial and temporal components of the spike-triggered average as described previously (Petrusca et al., 2007). Parameters of these fits (e.g. receptive field radius, time course principal components) were used for cell type classification in combination with additional parameters such as spike time autocorrelation and mosaic arrangement of receptive fields. Correspondences between functionally defined RGC types and the morphologically distinct parasol, midget and small bistratified cells were inferred based on cell densities and light response properties, as described previously (Field et al., 2007).

High resolution spatial receptive fields shown in Figs. 1A, 2, 3, and 6A were calculated by collapsing the spike-triggered average over time. For this purpose, the time course was calculated from the average of a subset of stimulus pixels whose absolute peak intensity was 3.5 times the robust standard deviation of all pixel intensities.

Cone mapping and single cone stimulation

Cone locations were calculated by combining high resolution receptive field maps obtained from hundreds of RGCs, using one of two methods. The first method was derived from first principles of Bayesian estimation, the second was a rapid *ad hoc* algorithm useful for real time analysis in closed-loop experiments with time limits. The two methods yielded similar but not identical cone maps.

The first method was to fit a parametric cone location model so as to maximize the likelihood across all recorded cell spike train data simultaneously, as described previously (Field et al., 2010). After building a map of cone locations maximizing the likelihood over the data (e.g. Fig. 1B), final cone locations were selected by a greedy algorithm that incorporated both the incremental improvement in likelihood for each added cone as well as priors implementing an exclusion radius around each cone. The cutoff to stop the greedy addition of cones was chosen manually for each cone map.

The second method for cone location mapping was a stepwise approach. This followed the previously described confirmatory approach (Field et al., 2010), except that instead of fitting cone locations to each RGC receptive field independently and then culling duplicates obtained from different RGCs, the current method first combined the significant pixels from all receptive fields into a single sensitivity map. Cone locations were then determined as local maxima of the sensitivity map as described previously. In practice, this method had the advantage of being faster than the Bayesian model fitting described above. It was also not as sensitive to regional variations in the quality of receptive field data, which on some data sets would leave the greedy model fitting approach unable to locate cones in a weaker receptive field area without first adding spurious cones into stronger areas (Sadeghi et al., 2013).

Both cone location analyses generated stimulus screen coordinates for the center of every cone found in the mosaic. These coordinates were used to specify regions of the screen

selected to stimulate single cones, as follows. Depending on cone spacing in each preparation, spots of radius 7.65–9.35 μm were generated around each cone center location. The full native screen resolution was used (pixels 1.7 μm on a side). For cases in which cone spacing was close enough that the resulting regions would overlap (e.g. Fig. 2 lower left panels, Fig. 4A ON midget cell), pixels were assigned to whichever competing cone had the nearest center coordinates. Single cones were then stimulated with uniform contrast steps over the defined regions. Recording trials were 750 ms long with the stimulus presentation occurring in the first 250 ms. Stimulation region (i.e. choice of cone) and contrast were randomized across trials.

In most cases, cones selected for individual stimulation were among the strongest cones in the receptive field as determined by an automated online analysis. In some cases, cones were manually selected for stimulation based on other criteria such as cone spacing, probability of divergence to multiple RGCs, or other goals independent of the current study. In some cases, cones selected for stimulation of one RGC were later found to provide good response data for another overlapping RGC. No significant differences were observed in the results from these different cone selection methods. In Fig. 6 (see below) every cone detected in each receptive field was individually stimulated.

Raster analyses

Raster plots for particular region/contrast combinations (Figs. 2, 3) were generated based on the spike times relative to stimulus onset across trials, with peristimulus time histograms (bin width 50 ms) indicating average firing rate over time within a trial. Discriminability indices, d', for single trial responses were calculated as the difference between the mean spike count in an interval 50–250 ms after flash onset versus the mean spike count over an equal interval in trials with no flash, divided by the average of the standard deviations of spike counts from the two conditions.

Response as a function of contrast was based on either the peak firing rate (Fig. 5), or the average number of spikes within a response window 50–250 ms after stimulus onset (Figs. 4, 6). To estimate peak firing rates, spike rasters were binned at 5 ms resolution and then smoothed with a Gaussian filter with a width approximately equal to the typical interspike interval (30 ms).

Univariance of contrast-response functions (Fig. 4) was assessed in RGCs by delivering a contrast series to four selected strong cones in the receptive field. The four contrast-response functions were allowed to scale freely on the contrast axis and were simultaneously fit to a single cumulative Gaussian function with a fixed mean (reversed as appropriate for OFF cells). The scale factors that minimized the squared deviations between the four curves and the template were then used to plot the curves overlaid on each other. For each RGC, the goodness of the overlay was quantified as the root-mean-square deviation between the contrast scaled data and the template, normalized by the cell's maximal observed response amplitude (Fig. 4B). In a few cases where the RGC gave negligible response to the weakest of the selected cones, that cone was excluded from the residuals analysis.

Estimates of RGC contrast-response functions for stimulation of the full receptive field center (Fig. 5) were generated as follows. For each RGC, a contrast series was delivered to a single cone, producing a contrast-response function (Fig. 5A). The contrast axis was then scaled by the ratio of the input strength of the selected cone versus the summed input strength of all the cones in the receptive field center, obtained from the receptive field map under spatiotemporal noise stimulation (e.g. Fig. 2, and see Fig. 6). Cone input strengths were calculated by summing the pixel intensity in the region surrounding each cone center location (Fig. 6A). The cones comprising the receptive field center were defined as those

within a 2.5–3 SD radius of the midpoint of the Gaussian fit of the receptive field, with an integrated pixel intensity > 1–1.5 robust SDs different from the background intensity and with the appropriate polarity. For most RGCs tested this analysis was repeated using several (1–4) different individual cones as the starting point, with similar results (not shown). For simplicity, Fig. 5 shows only the results based on the strongest cone tested for each RGC.

Relative strength of different cone inputs to RGCs (Fig. 6) were estimated using the rescaling factors that minimized the squared deviation between the contrast-response functions of individual cones (e.g. Fig. 4A). These measures were compared to cone input strength obtained by summing pixel intensities over the single cone stimulation regions in receptive field maps obtained using spatiotemporal noise stimulation. To visualize this correspondence, the stimulus regions were replotted with grey scale shading according to the input strength calculated by each method (Fig. 6B–F). Because the input strength measures obtained from spatiotemporal noise are relative rather than absolute, an arbitrary scaling was required to compare the two. For this purpose, the maximum value of the inputs strengths obtained from single cone stimulation was normalized to minimize the squared deviation from the strengths obtained from spatiotemporal noise. The two strength measures were then plotted against each other for each cone (Fig. 6G).

Acknowledgments

References

Ala-Laurila P, et al. Cone photoreceptor contributions to noise and correlations in the retinal output. Nat Neurosci. 2011

Baden T, et al. Spikes in mammalian bipolar cells support temporal layering of the inner retina. Curr Biol. 2013; 23:48–52. [PubMed: 23246403]

Baylor DA, Fettiplace R. Transmission from photoreceptors to ganglion cells in turtle retina. J Physiol. 1977; 271:391–424. [PubMed: 200736]

Baylor DA, et al. Spectral sensitivity of cones of the monkey Macaca fascicularis. J Physiol. 1987; 390:145–160. [PubMed: 3443931]

Bolinger D, Gollisch T. Closed-loop measurements of iso-response stimuli reveal dynamic nonlinear stimulus integration in the retina. Neuron. 2012; 73:333–346. [PubMed: 22284187]

Chichilnisky EJ, Baylor DA. Receptive-field microstructure of blue-yellow ganglion cells in primate retina. Nat Neurosci. 1999; 2:889–893. [PubMed: 10491609]

Chichilnisky EJ. A simple white noise analysis of neuronal light responses. Network: Computation in Neural Systems. 2001; 12:199–213.

Chichilnisky EJ, Kalmar RS. Functional asymmetries in ON and OFF ganglion cells of primate retina. J Neurosci. 2002; 22:2737–2747. [PubMed: 11923439]

Chun MH, et al. The synaptic complex of cones in the fovea and in the periphery of the macaque monkey retina. Vision Res. 1996; 36:3383–3395. [PubMed: 8977005]

Croner LJ, Kaplan E. Receptive fields of P and M ganglion cells across the primate retina. Vision Res. 1995; 35:7–24. [PubMed: 7839612]

Dawis S, et al. The receptive field organization of X-cells in the cat: spatiotemporal coupling and asymmetry. Vision Res. 1984; 24:549–564. [PubMed: 6740975]

Demb JB, et al. Functional circuitry of the retinal ganglion cell's nonlinear receptive field. J Neurosci. 1999; 19:9756–9767. [PubMed: 10559385]

DeVries SH. Bipolar cells use kainate and AMPA receptors to filter visual information into separate channels. Neuron. 2000; 28:847–856. [PubMed: 11163271]

Devries SH, Baylor DA. Mosaic arrangement of ganglion cell receptive fields in rabbit retina. J Neurophysiol. 1997; 78:2048–2060. [PubMed: 9325372]

Enroth-Cugell C, et al. Spatio-temporal interactions in cat retinal ganglion cells showing linear spatial summation. J Physiol. 1983; 341:279–307. [PubMed: 6620181]

Field GD, et al. Functional connectivity in the retina at the resolution of photoreceptors. Nature. 2010; 467:673–677. [PubMed: 20930838]

Field GD, et al. Retinal processing near absolute threshold: from behavior to mechanism. Ann Revs Physiol. 2005; 67

Field GD, et al. Spatial properties and functional organization of small bistratified ganglion cells in primate retina. J Neurosci. 2007; 27:13261–13272. [PubMed: 18045920]

Frechette ES, et al. Fidelity of the ensemble code for visual motion in primate retina. J Neurophysiol. 2005; 94:119–135. [PubMed: 15625091]

Gauthier JL, et al. Receptive fields in primate retina are coordinated to sample visual space more uniformly. PLoS Biol. 2009; 7:e63.

Gouras P. Identification of cone mechanisms in monkey ganglion cells. J Physiol. 1968; 199:533–547. [PubMed: 4974745]

Gouras P, Zrenner E. Enhancement of luminance flicker by color-opponent mechanisms. Science. 1979; 205:587–589. [PubMed: 109925]

Grunert U, et al. Immunocytochemical analysis of bipolar cells in the macaque monkey retina. J Comp Neurol. 1994; 348:607–627. [PubMed: 7530731]

Hochstein S, Shapley RM. Linear and nonlinear spatial subunits in Y cat retinal ganglion cells. J Physiol. 1976; 262:265–284. [PubMed: 994040]

Hofer H, et al. Organization of the human trichromatic cone mosaic. J Neurosci. 2005; 25:9669–9679. [PubMed: 16237171]

Hornstein EP, et al. Electrical coupling between red and green cones in primate retina. Nat Neurosci. 2004; 7:745–750. [PubMed: 15208634]

Kaplan E, et al. New views of primate retinal function. Progress in retinal research. 1990; 9

Kaplan E, Shapley RM. The primate retina contains two types of ganglion cells, with high and low contrast sensitivity. Proc Natl Acad Sci U S A. 1986; 83:2755–2757. [PubMed: 3458235]

Kolb H, Marshak D. The midget pathways of the primate retina. Doc Ophthalmol. 2003; 106:67–81. [PubMed: 12675488]

Kuffler SW. Discharge patterns and functional organization of mammalian retina. J Neurophysiol. 1953; 16:37–68. [PubMed: 13035466]

Lee BB, et al. Sensitivity of macaque retinal ganglion cells to chromatic and luminance flicker. J Physiol. 1989; 414:223–243. [PubMed: 2607430]

Litke AM, et al. What does the eye tell the brain?: Development of a system for the large-scale recording of retinal output activity. Nuclear Science, IEEE Transactions on. 2004; 51:1434–1440.

Marmarelis, PZ.; Marmarelis, VZ. Analysis of Physiological Systems: the White-noise Approach. New York: Plenum Press; 1978.

Menzel, R.; Snyder, AW. Introduction to Photoreceptor Optics—An Overview. In: Snyder, AW.; Menzel, R., editors. Photoreceptor Optics. Berlin, Heidelberg: Springer Berlin Heidelberg; 1975. p. 1-13.

Naka KI, Rushton WA. An attempt to analyse colour reception by electrophysiology. J Physiol. 1966a; 185:556–586. [PubMed: 5918059]

Naka KI, Rushton WA. S-potentials from colour units in the retina of fish (Cyprinidae). J Physiol. 1966b; 185:536–555. [PubMed: 5918058]

Nassi JJ, Callaway EM. Parallel processing strategies of the primate visual system. Nat Rev Neurosci. 2009; 10:360–372. [PubMed: 19352403]

Petrusca D, et al. Identification and characterization of a Y-like primate retinal ganglion cell type. J Neurosci. 2007; 27:11019–11027. [PubMed: 17928443]

Rodieck, RW. The First Steps in Seeing. Sunderland, MA: Sinauer; 1998.

Sadeghi K, et al. Monte Carlo methods for localization of cones given multielectrode retinal ganglion cell recordings. Network. 2013; 24:27–51. [PubMed: 23194406]

Schneeweis DM, Schnapf JL. Photovoltage of rods and cones in the macaque retina. Science. 1995; 268:1053–1056. [PubMed: 7754386]

Schwartz GW, et al. The spatial structure of a nonlinear receptive field. Nat Neurosci. 2012; 15:1572–1580. [PubMed: 23001060]

Shapley RM, Victor JD. How the contrast gain control modifies the frequency responses of cat retinal ganglion cells. J Physiol. 1981; 318:161–179. [PubMed: 7320887]

Sincich LC, et al. Resolving single cone inputs to visual receptive fields. Nat Neurosci. 2009; 12:967–969. [PubMed: 19561602]

Smith VC, et al. Responses of macaque ganglion cells to the relative phase of heterochromatically modulated lights. J Physiol. 1992; 458:191–221. [PubMed: 1302264]

Snyder, AW. Photoreceptor Optics—Theoretical Principles. In: Snyder, AW.; Menzel, R., editors. Photoreceptor Optics. Berlin, Heidelberg: Springer Berlin Heidelberg; 1975. p. 38-55.

Soo FS, et al. Fine spatial information represented in a population of retinal ganglion cells. J Neurosci. 2011; 31:2145–2155. [PubMed: 21307251]

Sterling, P.; Demb, JB. Retina. In: Shepherd, GM., editor. The synaptic organization of the brain. New York: Oxford University Press; 2004. p. 217-269.

Victor JD, Shapley RM. The nonlinear pathway of Y ganglion cells in the cat retina. J Gen Physiol. 1979; 74:671–689. [PubMed: 231636]

Wassle H. Parallel processing in the mammalian retina. Nat Rev Neurosci. 2004; 5:747–757. [PubMed: 15378035]

Wassle H, et al. Immunocytochemical characterization and spatial distribution of midget bipolar cells in the macaque monkey retina. Vision Res. 1994; 34:561–579. [PubMed: 8160377]
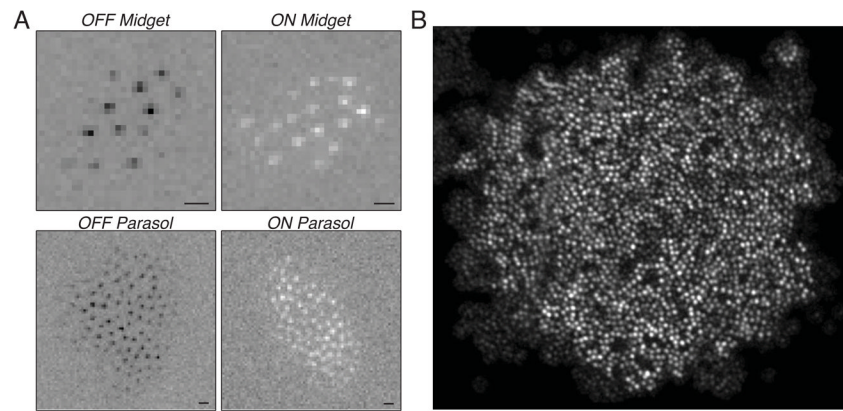
Figure 1. Mapping cone locations using high resolution spatiotemporal noise stimuli
A, High resolution receptive field maps from primate retinal ganglion cells of the four numerically dominant types, obtained by reverse correlation with spatiotemporal noise stimuli. Punctate islands of sensitivity in the receptive fields reveal the locations of individual cone photoreceptors (Field et al., 2010). Stimulation was from the ganglion cell side of the retina, so cone receptive fields reflect inner segment light guide and waveguide properties (Menzel and Snyder, 1975; Snyder, 1975). Scale bars, 15 µm. **B**, Map of full cone mosaic obtained over the hexagonal recording array. Receptive field data from hundreds of RGCs were combined to fit a model of punctate spatial inputs that maximized the likelihood over recorded spike trains (Field et al., 2010). Intensity at each putative cone location indicates its incremental contribution to likelihood. Brighter cones are generally 1) those detected in the receptive fields of multiple overlapping RGCs, 2) those obtained from receptive fields exhibiting highest signal-to-noise, and 3) those providing strongest input to RGCs. Scale bar, 100 µm.
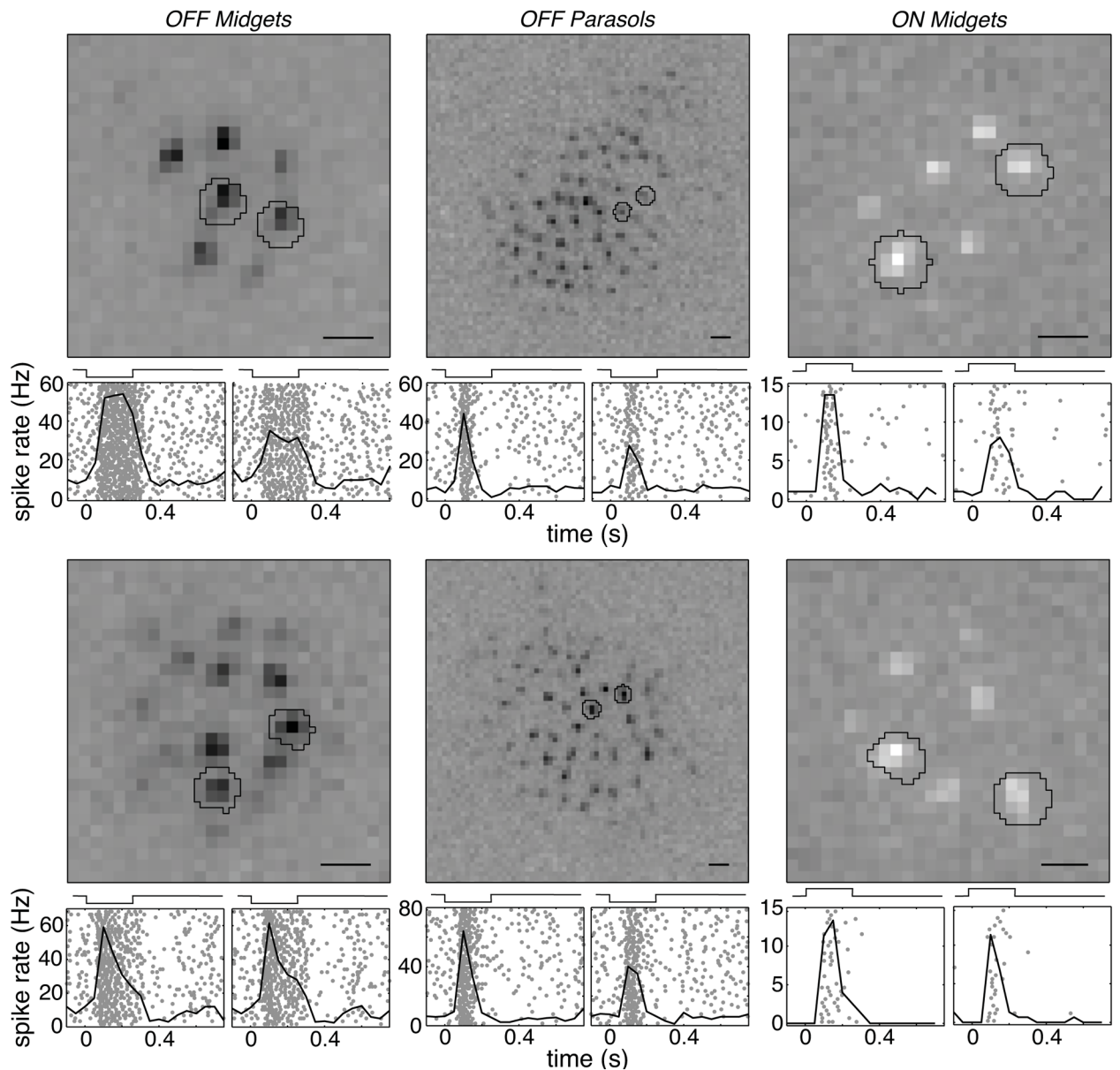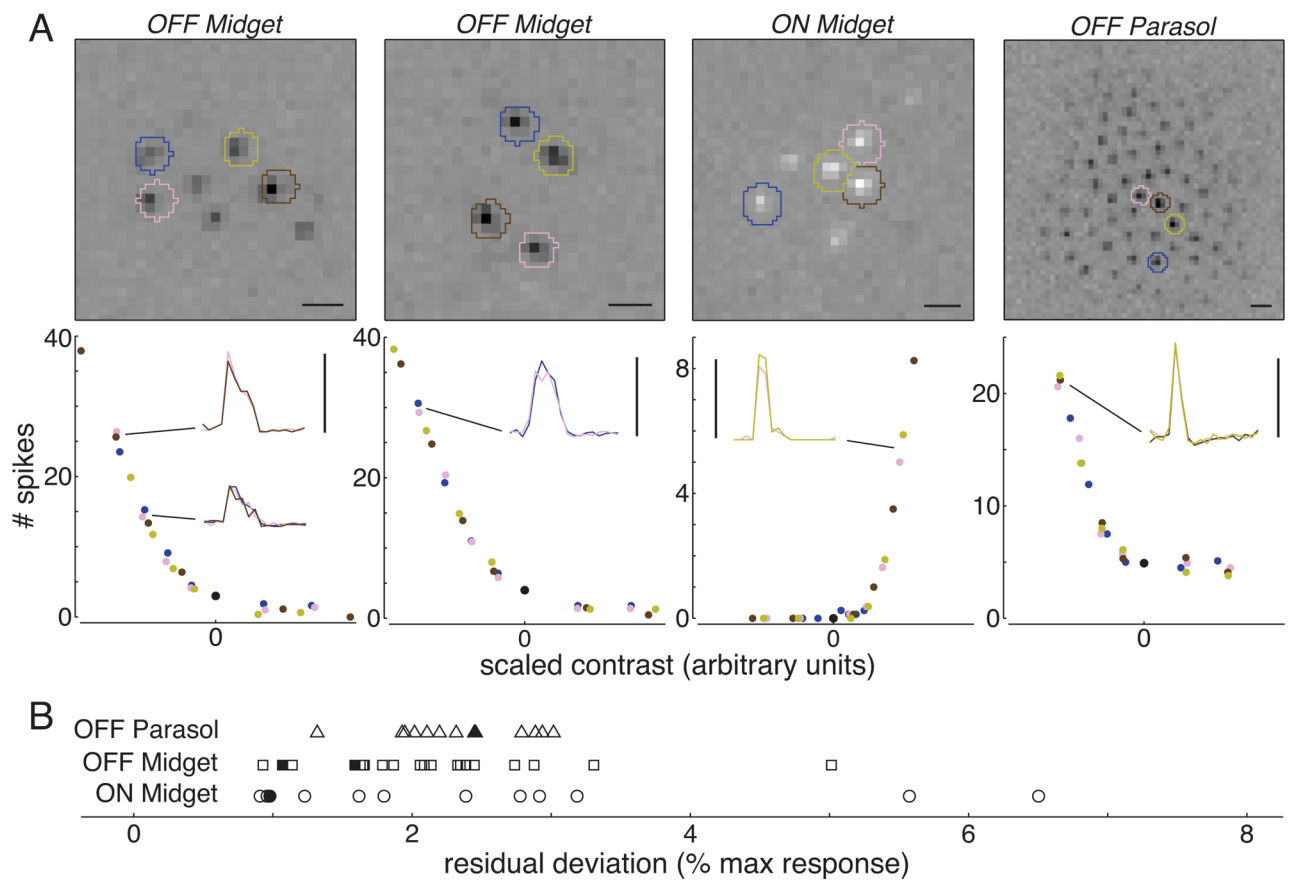
**Figure 2. Ganglion cell responses to single cone stimulation**

Three of the numerically dominant RGC types responded robustly to single cone stimulation. In each high resolution receptive field map, two stimulus regions are indicated by black polygonal outlines, with each region selected to activate a single cone in isolation. Scale bars 15 μm. Responses to stimulation of each region separately are plotted below as rasters over 40–50 trials (rows of grey dots) and peristimulus time histograms (black traces). For each RGC, the left raster plot corresponds to the leftmost stimulus region. The stimulus was a contrast step 0–250 ms (indicated above response plot). For the OFF cells, the stimulus was a 96% contrast decrement and for the ON cells it was an increment. Discriminability indices, d' (see Experimental Procedures), for single-trial responses to stimulation of the stronger (leftmost) stimulus region in each RGC were 6.9 and 5.5 for the top and bottom OFF midgets respectively; 2.9 and 5.3 for the OFF parasols; and 2.6 and 3.9 for the ON midgets.

Figure 3. Divergence of signals from a single cone to multiple ganglion cells
Receptive field maps are shown for four RGCs recorded simultaneously, along with their
responses to stimulation of the single indicated cone (solid black outline). Dotted or dashed
fiducial outlines show boundaries of the receptive field center region for all four RGCs. The
stimulated cone elicits opposite polarity responses in the receptive field surround region of
multiple nearby RGCs, e.g. lower right panel. Scale bars 15 μm.

Figure 4. Univariance of cone inputs to midget and parasol cells
A, For each RGC, four cone stimulus regions were selected (colored outlines, top panels), and responses were recorded to a series of contrast steps. Bottom panels show the average number of spikes recorded during stimulation as a function of stimulus contrast (colored points). This function was scaled separately for each cone along the contrast axis so as to align the four functions (see Experimental Procedures). Black point represents baseline response with no stimulus. Response time courses corresponding to groups of points with similar response amplitudes are shown as colored traces. Vertical scale bars for the time course traces correspond to 10 Hz for the ON midget RGC and 40 Hz for the other RGCs. Scale bars for receptive field maps, 15 μm. **B**, For each of 47 RGCs tested (13 OFF Parasols, 22 OFF Midgets, 12 ON Midgets), the residual deviation (see Experimental Procedures) after scaling of the individual cone contrast response functions is plotted as a percentage of the maximum response amplitude. Filled symbols are the RGCs shown in (A).
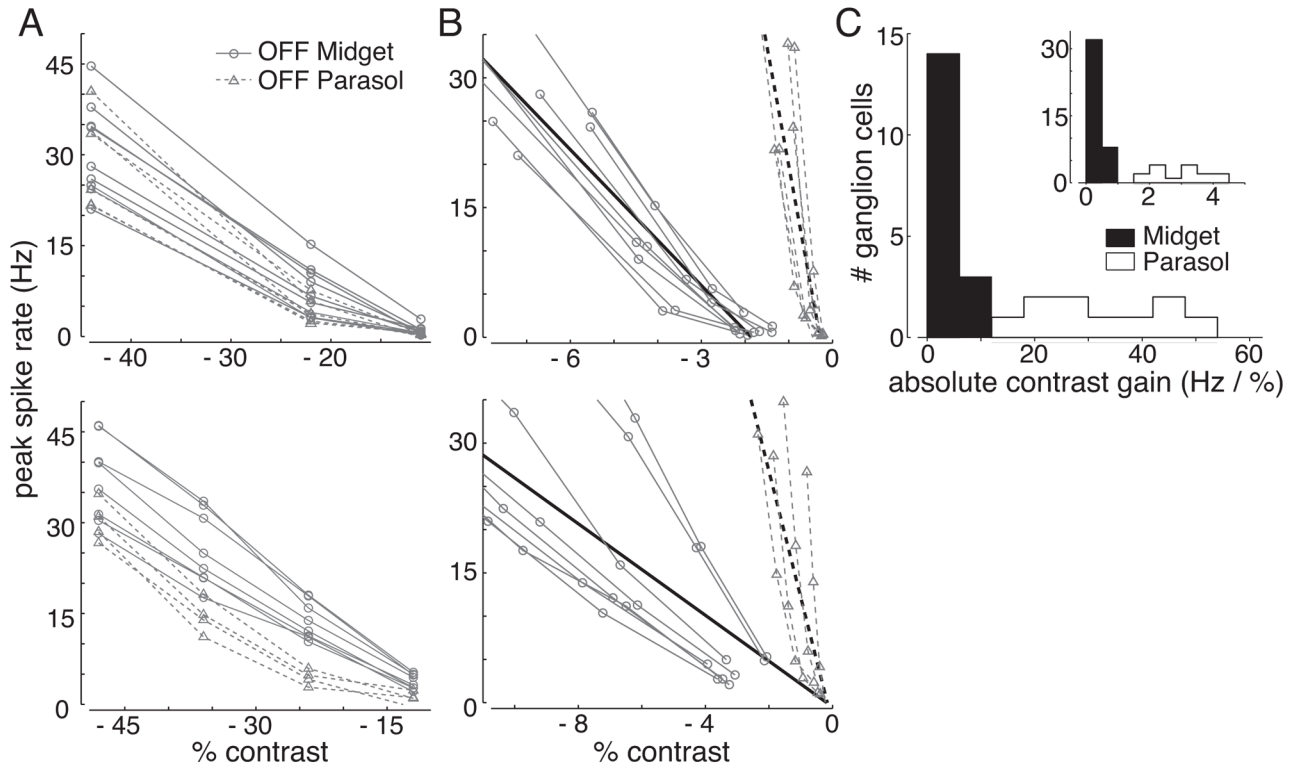
Figure 5. Contrast gain of midget and parasol cells
A, Contrast-response functions for simultaneously recorded OFF midget and OFF parasol RGCs. Data from two preparations are shown in separate rows. Peak firing rates are shown from responses to 250 ms steps of light of increasing contrast presented in single cone stimulation regions (see Fig. 2). Each trace represents responses of a single midget (solid lines with circles) or parasol (dashed lines with triangles) cell to stimulation of a single cone. **B**, Estimated contrast-response of cells in (A) to stimulation of the full receptive field center, obtained by scaling the contrast-response curve measured for a single cone by its fractional cone input strength, obtained from receptive field maps (see Experimental Procedures). Linear fits are plotted for the collection of midget (heavy solid line) and parasol (heavy dashed line) cells. **C**, Distribution of contrast gains in individual midget and parasol cells, estimated from the slopes of linear fits to each trace in (B). Inset replots the contrast gain distribution of putative midget and parasol cells in response to drifting sinusoidal gratings (Kaplan and Shapley, 1986).
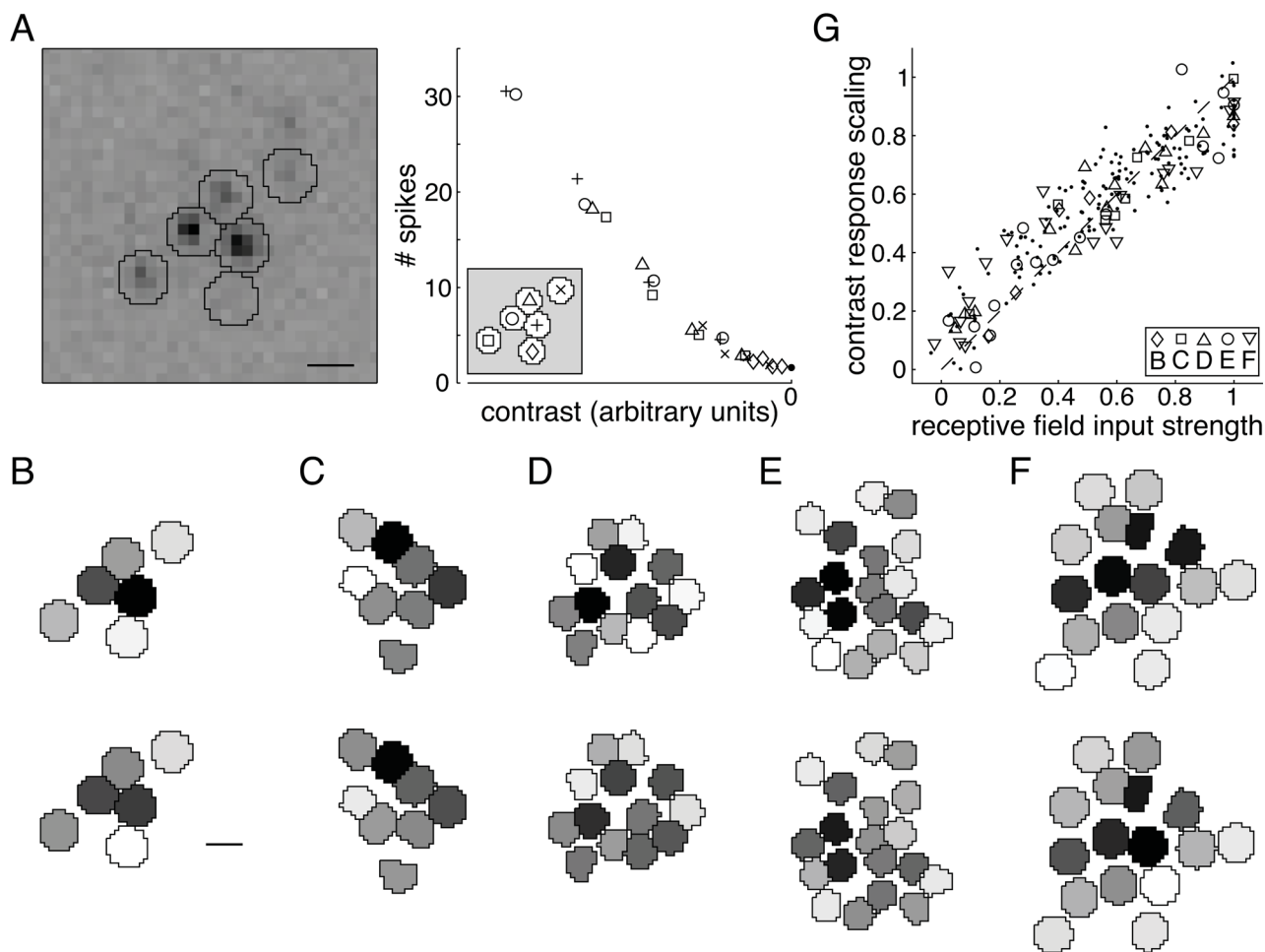
Figure 6. Comparison of cone input strength estimates
A, Two methods for estimating the strength of individual cone inputs. Left, the high resolution spatial receptive field map of an OFF midget RGC with six selected stimulus regions outlined. Scale bar 15 μm. Right, contrast-response functions for the six indicated regions stimulated with a series of 250 ms contrast decrements, rescaled on the contrast axis so as to overlay. Responses to stimulation of different cones are plotted with different symbols, key is inset. **B**, Comparison of cone input strengths calculated by the two methods for the cell in (A). Top, strength of each cone input obtained by integrating the receptive field map intensity within each cone stimulation region. Bottom, strength of cone input obtained from the scaling required to overlay the contrast-response functions of all cones. Scale bar, 15 μm, applies to panels (B–F). **C–F**, as in (B), for four additional OFF midget cells. **G**, Cone input strengths estimated by the two methods in (A), plotted against each other for every cone in 21 OFF midget receptive fields. Key to symbols for cells from panels (B–F) inset, additional cells are points. Dashed line represents equality.